AMERICAN SOCIETY FOR MICROBIOLOGY | Journal of Virology®

GENOME REPLICATION AND REGULATION OF VIRAL GENE EXPRESSION

The Epstein-Barr Virus Enhancer Interaction Landscapes in Virus-Associated Cancer Cell Lines

Weiyue Ding,[a] Chong Wang,[a] Yohei Narita,[a] Hongbo Wang,[a] Merrin Man Long Leong,[a] Alvin Huang,[a] Yifei Liao,[a] Xuefeng Liu,[b] Yusuke Okuno,[c] Hiroshi Kimura,[d] Benjamin Gewurz,[a] Mingxian Teng,[e] Shuilin Jin,[f] Yoshitaka Sato,[d] Bo Zhao[a]

[a]Division of Infectious Diseases, Department of Medicine, Brigham and Women's Hospital, Harvard Medical School, Boston, Massachusetts, USA
[b]Comprehensive Cancer Center, Ohio State University, Columbus, Ohio, USA
[c]Department of Virology, Nagoya City University Graduate School of Medicine, Nagoya, Aichi, Japan
[d]Department of Virology, Nagoya University Graduate School of Medicine, Nagoya, Aichi, Japan
[e]Department of Biostatistics and Bioinformatics, H. Lee Moffitt Cancer Center and Research Institute, Tampa, Florida, USA
[f]Precision Neurology Program, Brigham and Women's Hospital, Harvard Medical School, Boston, Massachusetts, USA

Weiyue Ding, Chong Wang, and Yohei Narita are co-first authors. Author order was determined by the corresponding author after negotiation.

ABSTRACT Epstein-Barr virus (EBV) persists in human cells as episomes. EBV episomes are chromatinized and their 3D conformation varies greatly in cells expressing different latency genes. We used HiChIP, an assay which combines genome-wide chromatin conformation capture followed by deep sequencing (Hi-C) and chromatin immunoprecipitation (ChIP), to interrogate the EBV episome 3D conformation in different cancer cell lines. In an EBV-transformed lymphoblastoid cell line (LCL) GM12878 expressing type III EBV latency genes, abundant genomic interactions were identified by H3K27ac HiChIP. A strong enhancer was located near the BILF2 gene and looped to multiple genes around BALFs loci. Perturbation of the BILF2 enhancer by CRISPR interference (CRISPRi) and CRISPR activation (CRISPRa) altered the expression of BILF2 enhancer-linked genes, including BARF0 and BALF2, suggesting that this enhancer regulates the expression of linked genes. H3K27ac ChIP followed by deep sequencing (ChIP-seq) identified several strong EBV enhancers in T/NK (natural killer) lymphoma cells that express type II EBV latency genes. Extensive intragenomic interactions were also found which linked enhancers to target genes. A strong enhancer at BILF2 also looped to the BALF loci. CRISPRi also validated the functional connection between BILF2 enhancer and BARF1 gene. In contrast, H3K27ac HiChIP found significantly fewer intragenomic interactions in type I EBV latency gene-expressing primary effusion lymphoma (PEL) cell lines. These data provided new insight into the regulation of EBV latency gene expression in different EBV-associated tumors.

IMPORTANCE EBV is the first human DNA tumor virus identified, discovered over 50 years ago. EBV causes ~200,000 cases of various cancers each year. EBV-encoded oncogenes, noncoding RNAs, and microRNAs (miRNAs) can promote cell growth and survival and suppress senescence. Regulation of EBV gene expression is very complex. The viral C promoter regulates the expression of all EBV nuclear antigens (EBNAs), some of which are very far away from the C promoter. Another way by which the virus activates remote gene expression is through DNA looping. In this study, we describe the viral genome looping patterns in various EBV-associated cancer cell lines and identify important EBV enhancers in these cells. This study also identified novel opportunities to perturb and eventually control EBV gene expression in these cancer cells.

KEYWORDS 3D genome organization, episome, Epstein-Barr virus, latency

Editor Lori Frappier, University of Toronto

Address correspondence to Bo Zhao, bzhao@bwh.harvard.edu, Shuilin Jin, sjin5@partners.org, or Yoshitaka Sato, yssato@med.nagoya-u.ac.jp.

The authors declare no conflict of interest.

Received 8 May 2022
Accepted 23 August 2022
Published 12 September 2022

Epstein-Barr virus (EBV) was the first human tumor virus discovered, identified from a case of Burkitt's lymphoma in Africa more than 50 years ago (1, 2). EBV is now linked to ~200,000 cases of various cancers each year (3). EBV is causally related to various B cell malignancies, including endemic Burkitt lymphoma, Hodgkin's lymphoma, and AIDS central nervous system lymphomas; nasopharyngeal carcinoma (NPC); ~10% of gastric cancers; and some T/NK (natural killer) cell lymphomas (3). In these EBV-associated cancers, EBV genomes persist as circularized viral episomes which can replicate and segregate with the host genome during mitosis (4, 5). Most of the cancer cells harbor latent viral genome.

EBV-related cancers express various types of EBV latency genes. There are three major types of EBV latency seen in these cancers. Epstein-Barr virus nuclear antigen (EBNA) 1, noncoding RNAs, EBV-encoded small RNAs (EBERs), and microRNAs are expressed in type I latency infected cells, including Burkitt's lymphoma and primary effusion lymphoma (PEL). EBNA1, latent membrane protein (LMP) 1/2, EBER, and microRNAs are expressed in type II latency cases, including NPC and T/NK cell lymphoma. All EBNAs, including LP, 1, 2, 3A-C, LMP1/2, EBER, and microRNAs, are expressed in type III latency infected cells. Type III latency is seen in posttransplant lymphoproliferative disease (PTLD) and AIDS central nervous system (CNS) lymphomas and EBV immortalized lymphoblastoid cell lines (LCLs) that develop from *in vitro* cell cultures (2). In these cancer cells, EBV episomes can dock with different host genomic sites. In type III latency, EBV episome tends to dock with active enhancer sites with high H3K27ac signals (6, 7). In type I latency, EBV episome tends to dock with repressed regions marked by H3K9me3 (7). Docking with regions enriched with different histone marks may be important for the expression of different latency genes.

EBNA1 is expressed in all EBV cancers, where it tethers the EBV episomes to the host DNA during mitosis, ensuring that the episomes are divided evenly among the daughter cells (8–12). EBNA2 and EBNALP activate the transcription of viral and host genes, including MYC (13, 14). EBNA3A and 3C represses CDKN2A loci to suppress senescence (15). LMP1 activates NF-κB to provide pro-survival signals to prevent cancer cell death (16). LMP2 can mimic B cell receptor (BCR) signaling to promoting malignant transformation (17). EBER can modulate innate immunity and host transcription factors (TF) such as PAX5 DNA binding (18–21). EBV microRNAs can inhibit apoptosis (22). Limited numbers of EBV lytic genes are also expressed in these cancers. The expression patterns vary significantly (23). The roles of these lytic genes in cancer development are still poorly defined.

Several enhancers are important in controlling the expression of EBV latency genes (24, 25). OriP is bound by multiple host TFs and functions as a strong enhancer that controls LMP1 expression (25, 26). The EBV episome is organized to facilitate efficient interactions between enhancers and their direct target genes, ensuring the expression of latency genes. The 3D organizations of EBV episomes vary greatly between type III latency and type I latency (27). CCCTC-binding factors (CTCF) can function as insulators preventing the spread of active chromatin marks (28). CTCF can also form dimers to bring distant DNA to close proximity, allowing remote enhancers to contact their direct target genes (29). Cohesin subunits RAD21, SMC1A, and SMC3 form a ringlike structure which encompasses the CTCF dimer to stabilize the loop (30). CTCF and cohesins bind to the EBV genome and divide it into function domains (25, 31–33). CTCF and RAD21 binding to the EBV genome vary greatly between type I and type III latency-expressing cells (27). Much higher CTCF and RAD21 ChIP-seq peaks are seen in cells expressing type I latency genes than in those expressing type III latency genes (27).

Chromatin conformation capture (3C)-based assays interrogate the 3D genomic interactions between different regions (34). 3C followed by deep sequencing (Hi-C) captures the genome-wide interactions between DNA regions (35). Captured Hi-C enriches the genome-wide interactions between a selected genomic region with the rest of the genome through selecting ligation products enriched by an oligonucleotide array of interested region (27). Captured Hi-C have been used to investigate the interactions between EBV enhancers and their direct target genes (36). HiChIP interrogates the genome-wide genomic DNA interaction enriched by a chromatin immune precipitation step (37, 38). Using H3K27ac HiChIP, we investigated the genome-wide interactions within the EBV genome in cells expressing three types of EBV latency genes.

RESULTS

3D genome organization of type III EBV latency gene expressing GM12878 LCL. We first investigated the EBV epigenome and 3D genome organization in cells expressing type III latency genes. The encyclopedia of DNA elements (ENCODE) GM12878 H3K27ac ChIP-seq data were analyzed by first mapping the sequencing reads to the B95.8 strain of EBV genome using Bowtie. MACS2 was used to identify significant peaks. The most prominent H3K27ac peak was around the BILF2 gene, and was about 3 kb wide. Other peaks were found near LMP1, LMP2A/B, Cp, OriP, and BARF1 (Fig. 1A). RNA-seq reads were mapped using STAR. The analysis found that type III latency genes EBNAs and LMPs were expressed. Abundant transcripts were also found at BHRL1, OriLyt, BMRF1, BALFs, BARF1, and BILF2 (Fig. 1A). ENCODE CTCF and cohesin subunit RAD21 ChIP-seq data were mapped to the EBV genome. CTCF and RAD21 bound strongly at a site between LMP1 and BARF1. Another strong CTCF peak was near BXRF1. The region between BXRF1 and BARF1 may be within a functional domain shielded by the CTCF/cohesin sites.

We then reanalyzed published GM12878 LCL H3K27ac HiChIP data for interactions within EBV episomes. For HiChIP assays, cells were first cross-linked by formaldehyde and lysed. Mbo I was used to cut DNA. The DNA ends were filled in with biotinylated nucleotides and ligated *in situ*. H3K27ac chromatin immunoprecipitation (ChIP) was used to enrich the DNA fragments with H3K27ac marks. Avidin beads were used to enrich the DNA fragments with the ligation products. Paired-end sequencing was used to identify the interacting genomic regions. Bowtie was used to map the sequencing reads against EBV sequence to identify the ligation products derived from the EBV genome. HiChIP interaction reads were counted between pairwise 1-kb bins of EBV genome. The count table, consisting of data from the 7 cell lines in this analysis (GM12878, KAI3, NUNK1, SNT-13, SNT-16, BC1, and JSC1), was normalized using the Voom tool with the "quantile" option to account for the sparsity and dispersion variations in count-based data. Circos plots were generated based on a normalized interaction frequency of 4 or higher, which accounted for the top ~5% of interactions. Abundant interactions between different EBV genomic regions were identified. The strongest interaction was between the strong enhancer at the BILF2 and the BALF5 or BARF1. The distances between BILF2 and BARF1 were ~18 kb, excluding the B958 deletion. BARF1 and BILF2/BdRF1 enhancers also interacted with many regions of the rest of EBV genome (Fig. 1A and B). Less frequent interactions between BILF2 enhancer and the genes on the opposite side of the BILF2 enhancer, including Cp, BHLF1, and Zp, were also evident, (Fig. 1B, lower part).

CRISPRi and CRISPRa were used to perturb the BILF2 enhancer to determine its activity in regulating the genes linked by HiChIP, including BALF2 and BARF0. Lentiviruses expressing dCAS9-KRAB-MeCP2 or dCAS9-VP64 were transduced into GM12878 LCLs and selected with blasticidin. Single guide RNA (sgRNA) targeting BILF2 enhancer or non-targeting control was packaged into lentiviruses and transduced into LCLs expressing stable dCAS9 fusion proteins. After puromycin selection, cells were grown for 2 days. Total RNAs were extracted from these cells. Reverse transcription-quantitative PCR (qRT-PCR) was used to measure the expression levels of BILF2 and BALF2. CRISPRi significantly repressed BILF2 ($P < 0.001$) and BALF2 expression ($P < 0.05$ or $P < 0.01$) (Fig. 1C). The CRISPRi did not affect the expression of nearby BILF1, while some sgRNAs increased BALF4 and BALF5 expression ($P < 0.05$) (Fig. S1A in the supplemental material). CRISPRa significantly increased BILF2 and BALF2 expression compared with the control sgRNA. CRISPRa had no effect on LMP1 expression (Fig. 1D). These data indicated that the linkage between BILF2 enhancer and gene in the BALF2 locus is functional. Perturbation of BILF2 enhancer affected the expression of genes linked by H3K27ac HiChIP.

3D genome organization of type II EBV latency gene expressing T/NK lymphoma cells. EBV-positive T/NK lymphomas are aggressive non-Hodgkin's lymphoma. RNA-seq analyses determined that these lymphomas express type II latency genes, including EBNA1, LMP1, LMP2A/2B, and EBER. In addition, the EBV lytic genes BNRF1, BILF1, BALF5/4/3/2, and BNLF2b were also detected in these patients (39–42). Interestingly, in the same cohort of patients, whole-exome sequencing found fewer mutations than in other lymphomas that are EBV-negative (39). In another study, EBV immediate early gene BZLF1 can be detected by qRT-PCRs in some T/NK lymphomas (40). To identify model cell lines faithfully represent the primary tumor samples, we analyzed the expression profiles of EBV positive T/NK

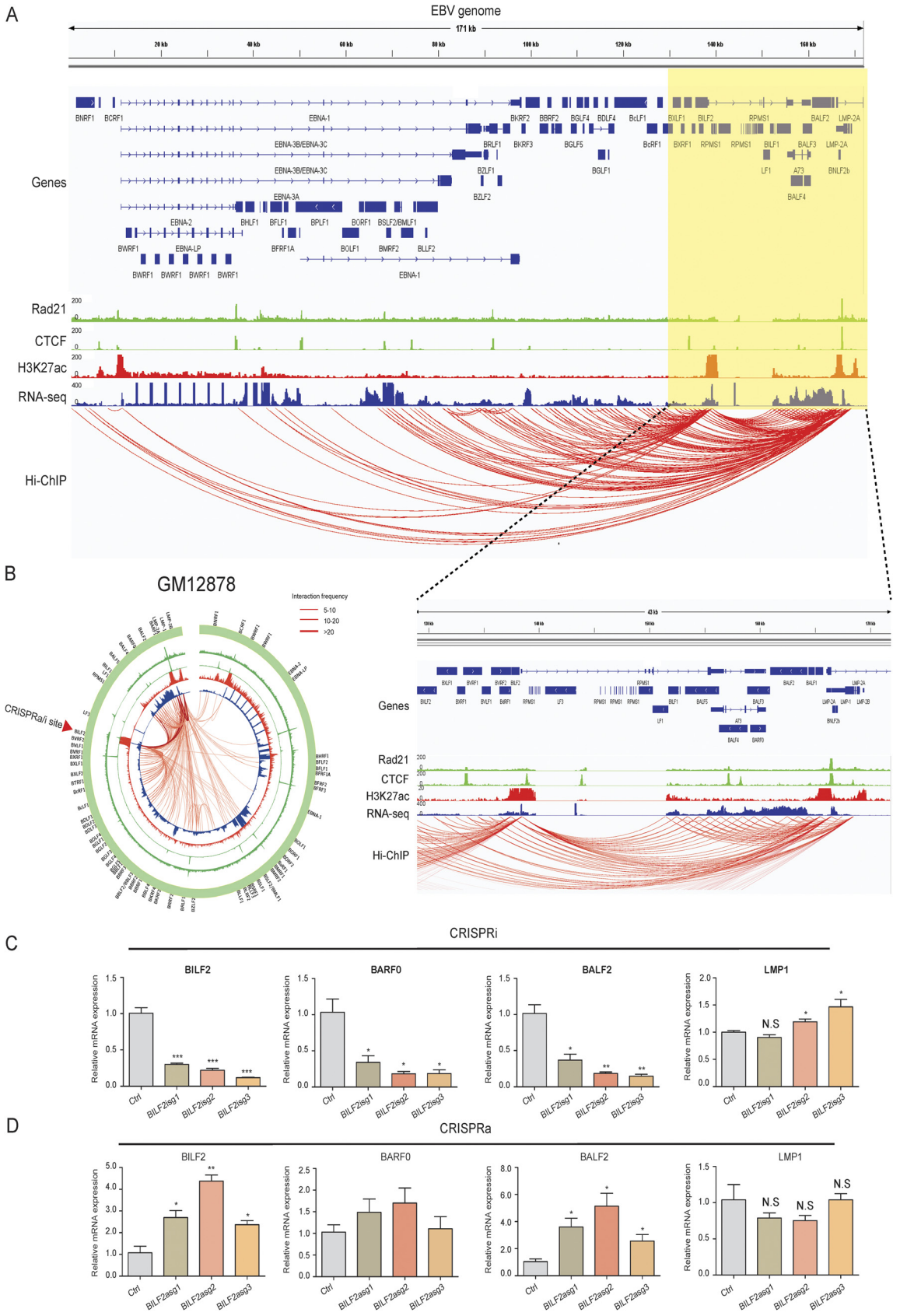

FIG 1 H3K27ac HiChIP interactions within the Epstein-Barr virus (EBV) genome in type III EBV latency cells. (A) GM12878 LCL H3K27ac HiChIP data were mapped to the EBV genome and visualized in IGV. DNA interactions are indicated by red arcs. ENCODE RAD21 (green, outside),

(Continued on next page)

lymphoma cell lines, including two NK lineage lymphoma cell lines KAI3 (43) and NUNK1, and two T cell lineage lymphoma cell line SNT13 and SNT16 (44) by RNA-seq. For KAI3 cells, type II latency genes were expressed (Fig. 2A). In addition, BILF2, LF1/2, BALF5/4/3, BARF1, BNLF2a/b were also expressed (Fig. 2A and S).

H3K27ac ChIP-seq was used to identify enhancers in EBV genome in KAI3 cells. Multiple enhancers in the EBV genome were identified. The major H3K27ac peak was located around BdRF1/BVRF2/BILF1. Other major peaks were around LMP1 and EBERs. Minor peaks were found around oriLyt, BNLF2a/b, and oriP (Fig. 2A and B).

H3K27ac HiChIP was used to connect enhancers to their direct target genes. In KAI3 cells, BILF2 enhancer frequently interacted with LF1/2, BALF5/4/3/2, and BARF1 regions (Fig. 2A and B). Furthermore, BILF2 enhancers frequently interacted with the rest of the EBV genome, suggesting that BILF2 enhancer functioned at an interaction hub within the EBV genome in type II latency (Fig. 2A and B).

CRISPRi was used to evaluate the functional significance of the loop between BILF2 enhancer and BARF1 expression. sgRNAs targeting the BILF2 enhancer or non-targeting control sgRNAs were packaged into lentiviruses and transduced into KAI3 cells stably expressing dCAS9-KRAB-MeCP2 fusion protein. After puromycin selection, total RNAs were extracted from these cells. qRT-PCR was used to evaluate the effect of CRISPRi on BARF1 expression. CRISPRi at BILF2 enhancer significantly repressed BARF1 expression ($P < 0.01$). CRISPRi also repressed BILF2 expression ($P < 0.01$ or $P < 0.05$) (Fig. 2C). These data indicated that BILF2 enhancer can regulate the expression of its direct target gene BARF1 through long-range enhancer looping.

Similar expression and enhancer interaction patterns were observed for NUNK1, SNT13 and SNT16 cells (Fig. 3A and B).

3D genome organization of type I EBV latency gene-expressing primary effusion lymphoma cells. The PEL cell lines BC1 and JSC express EBV type I latency genes. H3K27ac ChIP-seq of BC1 and JSC cells found peaks at the EBER loci, miRNA loci, and Qp, which drives the expression of EBNA1 in type I latency cells (45). H3K27ac HiChIP was used to evaluate the genome looping in these cells. Much less frequent interactions between BILF2 and the BALF gene cluster were found in BC1 and JSC cells. More frequent interactions were found between BILF2 and the genes on the opposite side (Fig. 4, bottom). We found no obvious enrichment of an anchor region that interacts with the rest of the genome (Fig. 4).

DISCUSSION

Enhancers play key roles in transcription regulation. One strong enhancer can control the expression of multiple genes. Enhancer can regulate the expression of genes from a distance by looping out the intervening DNA. Several strong enhancers have been identified in EBV episomes in cells expressing type III EBV latency genes (24). These enhancers can loop to their direct-target genes (31). The EBV episome looping patterns of type III and type I latency vary greatly, as determined by capture Hi-C that captures all the genomic interactions (27). Episomes in type III latency infected cells have a lot more intragenomic interactions than type I latency infected cells (27). HiChIP is a newly developed assay that detects genomic interactions enriched by specific protein markers, such as H3K27ac. Thus, H3K27ac HiChIP mostly captures active enhancer-enhancer or enhancer-promoter interactions. This new approach was used to detect intragenomic interactions within the EBV episomes in various cancer cell lines harboring EBV. Here, we provided new evidence that EBV episome looping in type II latency was similar to that in type III latency. The intragenomic interactions in cells with type I latency were similar in PEL and appeared to be random, lacking specific enrichment. In both type III and type II latency EBV-infected cells, very strong enhancers were

FIG 1 Legend (Continued)

CTCF (green, inside), H3K27ac ChIP-seq (red), and RNA-seq (blue) data were also mapped to the EBV genome and visualized in IGV. EBV annotation is shown on the top. The zoomed-in view on the right side of the EBV genome is shown under the main figure. (B) EBV episome is shown in circos plot. Red arrow indicates position of single guide RNA (sgRNA) for CRISPR interference (CRISPRi) or activation (CRISPRa). Normalized interaction frequency scale is shown on the top right. (C and D) GM12878 lymphoblastoid cell lines (LCLs) stably expressing (C) dCAS9-KRAB-MeCP2 or (D) dCAS9-VP64 were transduced with sgRNA expressing lentiviruses targeting BILF2 enhancer. After puromycin selection, total RNA was purified. Reverse transcriptase quantitative PCR (RT-qPCR) was used to evaluate the expression of BILF2, BALF2, and LMP1. Expression levels of non-targeting sgRNA-transduced cells were set at 1. *, $P < 0.05$; **, $P < 0.01$; ***, $P < 0.001$; NS, not significant.

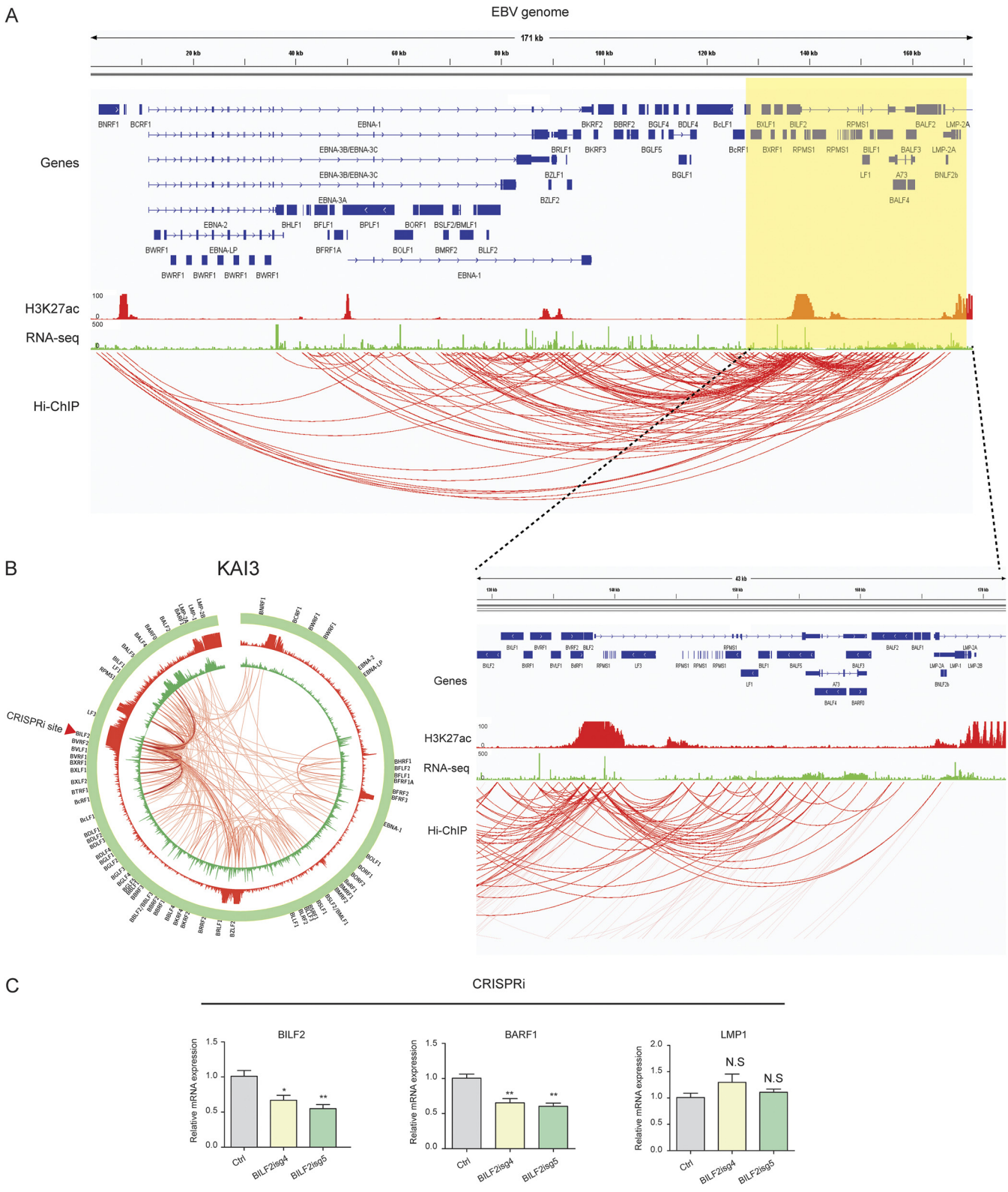

FIG 2 H3K27ac HiChIP interactions within the EBV genome in type II EBV latency cells. (A) EBV natural killer (NK) cell lymphoma KAI3 H3K27ac HiChIP data were mapped to the EBV genome and visualized in IGV. DNA interactions are indicated by red arcs. H3K27ac ChIP-seq and RNA-seq data were also mapped to the EBV genome and visualized in IGV. EBV annotation is shown on the top. Zoomed-in view on the right side of the EBV genome is shown under the main figure. (B) EBV episome is shown in circos plot. Red arrow indicates position of sgRNA for CRISPRi. Normalized interaction frequency scale is shown on the top right. (C) KAI3 cells stably expressing dCAS9-KRAB-MeCP2 were transduced with sgRNA-expressing lentiviruses targeting BILF2 enhancer. After puromycin selection, total RNA was purified. RT-qPCR was used to evaluate the expression of the BILF2 enhancer-linked genes BILF2 and BARF1. LMP1 which was away from the loops was used as control. Expression levels of non-targeting sgRNA-transduced cells were set at 1. *, $P < 0.05$; **, $P < 0.01$; NS, not significant.

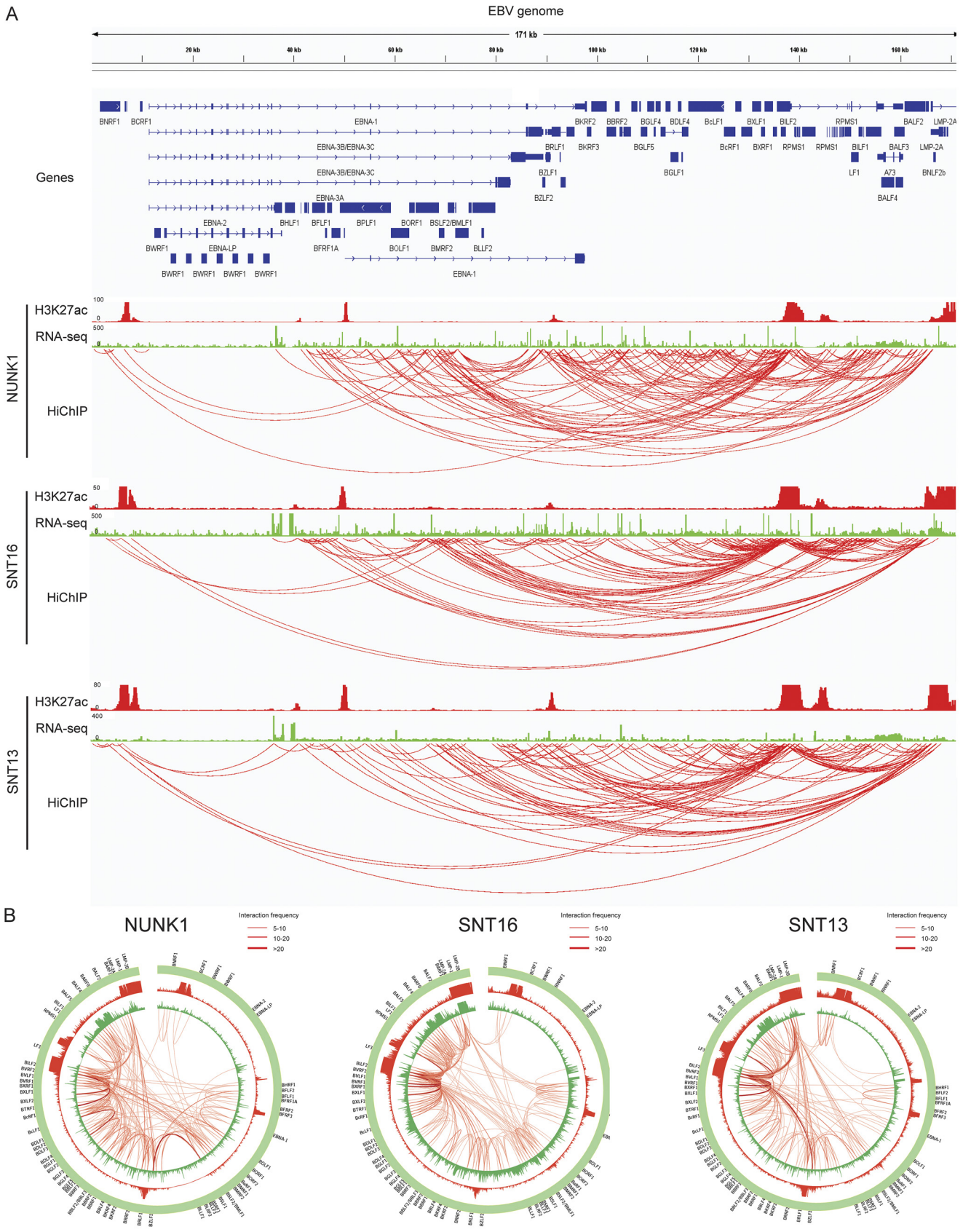

FIG 3 H3K27ac HiChIP interactions within the EBV genome in type II EBV latency cells NUNK, SNT13, and SNT16. (A) EBV T/NK cell lymphoma NUNK1, SNT13, and SNT16 H3K27ac HiChIP data were mapped to the EBV genome and visualized in IGV. DNA interactions are indicated by red arcs. H3K27ac ChIP-seq and RNA-seq data were also mapped to the EBV genome and visualized in IGV. EBV annotation is shown on the top. (B) EBV episome is shown in circos plot. Normalized interaction frequency scale is shown on the top right.

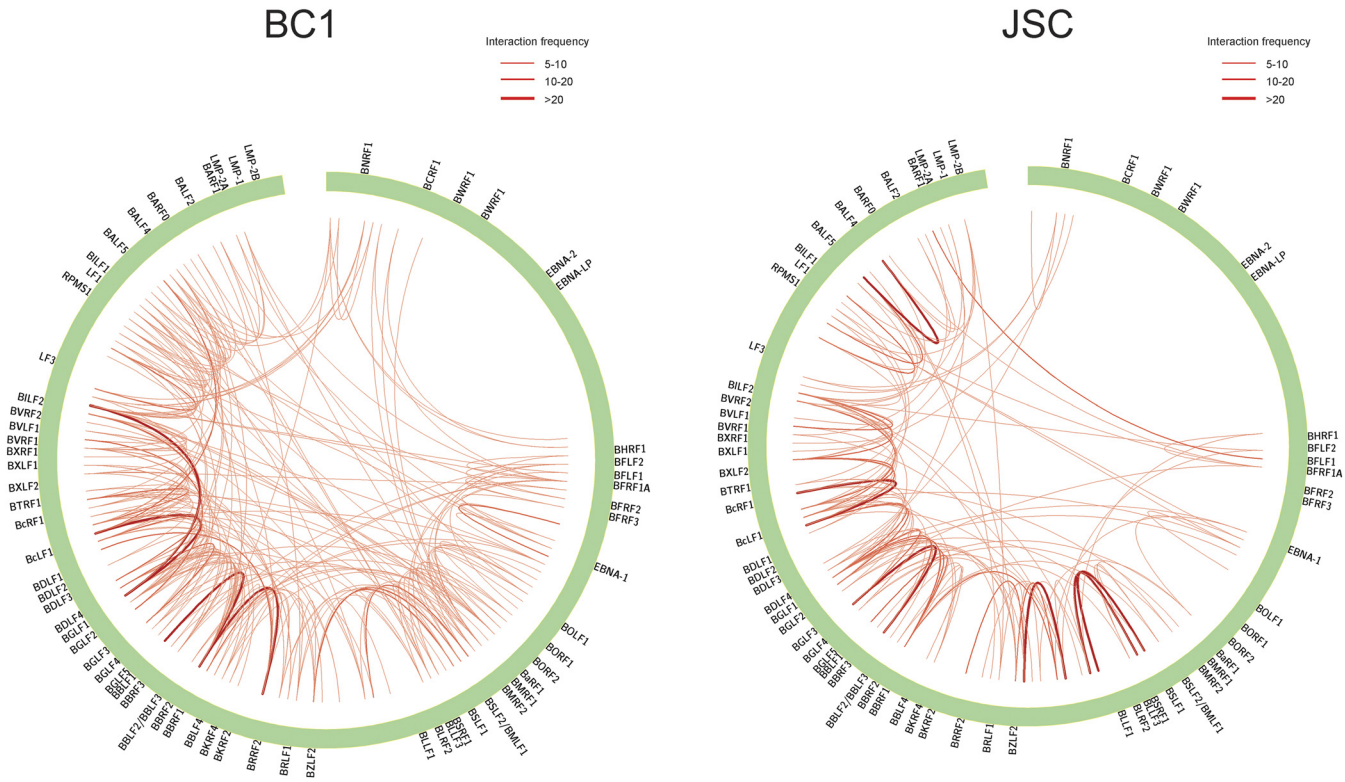

FIG 4 H3K27ac HiChIP interactions within the EBV genome in type I EBV latency cells BC1 and JSC. H3K27ac HiChIP data were mapped to the EBV genome and interactions are shown in circoplot. Normalized interaction frequency scale is shown on the top right.

present in the episomes. The frequent intragenomic interactions linking enhancers to their direct genes may be driven by these strong enhancers. In contrast, significantly fewer intragenomic interactions were found in type I latency cells, possibly due to the lack of strong enhancers and decreased EBV gene expression. Using CRISPRi, we confirmed the functional activity of a strong enhancer at the BILF2 locus, and perturbing this enhancer affected the expression of genes >20 kb away.

CTCF can function as an insulator, dividing the genome into different compartments. Enhancer-promoter interactions mostly occur within the same compartment. CTCF sites can prevent the spread of activation signals across the sites. CTCF can also form dimers while binding to its cognate DNA, bringing remote enhancers into close proximity to their direct-target genes. Cohesin proteins can form a ring and wrap around the DNA strands near CTCF dimers to further stabilize this interaction. In LCLs, a strong CTCF ChIP-seq peak resides between LMP1 and BARF1. A strong cohesion subunit RAD21 peak also overlaps with the CTCF peak. Another strong CTCF peak is localized at the left-hand side of the BILF2 enhancer. Stronger interactions within this CTCF marked domain were evident compared to the interaction between enhancers within the domain and sites outside the domain. CRISPRi at the BILF2 enhancer had no effect on LMP1, which is outside this CTCF domain, even though there were weak links between BILF2 enhancer and LMP1.

The distribution of EBV episomes in the nucleus is not random. In cells expressing type III latency genes such as LCL, EBV episomes dock to active enhancer regions (6, 7). Active enhancers can be enriched with many transcription factors and cofactors to form phase separated domains, ensuring high transcription activity. When EBV episomes are docked at these active sites, EBV enhancers can access enriched transcription factors and cofactors, allowing efficient transcription of enhancer targets. In cells expressing type I latency genes, such as Burkitt lymphoma cells, EBV episomes tends to dock to repressed chromatin (7). This can limit the available transcription cofactors for EBV enhancers; thus, only limited numbers of latency genes are expressed. Reducing episome enhancer-target interaction will further facilitate the silencing of EBV latency genes expressed in other latency types.

MATERIALS AND METHODS

Cells. EBV-positive NK/T cells KAI3, NUNK1, and SNT16 were cultured in Artemis medium 2 (Nihon Techno Service (NTS), Ushiku, Japan). NUNK1 cells were established from the peripheral blood of a 17-year-old boy suffering from NK-type chronic active EBV disease. NUNK1 cells were positive for CD56, HLA-DR, and CD2, but negative for CD20, CD21, CD3, CD4, and CD8. SNT13 was cultured in Artemis medium 2 supplemented with 700 U/mL IL-2. GM12878 was cultured in RPM1640 medium supplemented with 10% fetal bovine serum (FBS). 293T cells were maintained in Dulbecco's modified Eagle's medium with 10% FBS.

Ethics statement. Written informed consent was obtained from the parents of patients. The Institutional Review Board of Nagoya University Graduate School of Medicine approved this study.

HiChIP. HiChIP was performed according to described previously protocols (37). In brief, 10 million cells were harvested and cross-linked with 1% formaldehyde. Cells were lysed with Hi-C lysis buffer (10 mM Tris-HCl pH 7.5, 10 mM NaCl, 0.2% NP-40, 1× Roche protease inhibitors). DNA was digested by 375 U Mbo I (New England Biolabs [NEB] cat no. R0147M) at 37°C with shaking at 300 rpm for 2 h. DNA ends were filled in with biotin-dATP (Thermo Fisher Scientific cat no. 19524016), dCTP, dGTP, and dTTP mix, and DNA polymerase I, Klenow fragment (NEB, M0210) with shaking at 37°C for 1 h. Next, 4,000 U T4 DNA Ligase (NEB, M0202) was used for proximity DNA ligation with shaking at room temperature for 4 h followed by incubation at 16°C overnight. After ligation, DNA was sonicated using a Covaris M220. Fragmented DNAs were then diluted 10 times with ChIP dilution buffer (0.01% SDS, 1.1% Triton X-100, 1.2 mM EDTA, 16.7 mM Tris-HCl [pH 7.5], 167 mM NaCl) and samples were precleared with protein A Dynabeads at 4°C for 1 h. DNA-protein complexes were captured with 8 μL H3K27Ac antibody at 4°C overnight. DNA-protein complexes were captured with protein A beads with rotation at 4°C for 2 h. Beads were washed and DNAs were eluted twice with 150 μL of freshly prepared DNA elution buffer (50 mM sodium bicarbonate [pH 8.0], 1% SDS). The eluted DNA was reverse cross-linked. DNA was purified with a PCR purification kit (Qiagen, Hilden, Germany). Biotin dATP-labeled DNA was captured with 5 μL Streptavidin C-1 beads (Thermo Fisher, number 65001) and DNA was then transposed with 2.5 μL Tn5. Beads were then washed. After the final wash, beads were re-suspended with 23 μL double-distilled water, 25 μL 2× Phusion HF (New England Biosciences), and 1 μL each of Nextera forward primer (Ad1_noMX) and Nextera reverse primer (Ad2.X) at 12.5 μM. PCRs were run at: (i) 72°C for 5 min, (ii) 98°C for 1 min, (iii) 98°C for 15 s, (vi) 63°C for 30 s, and (v) repeat steps 1 to 4 for a total of 8 cycles, and final extension at 72°C for 1 min. After PCR amplification, a two-sided size selection with Ampure XP beads was performed for DNA size selection and purification. Samples were then sequenced on an Illumina NextSeq platform (2 × 75 bp).

ChIP-seq. CHIP-seq was performed following the methods of Zhao et al. (13). Cells were cross-linked with 1% formaldehyde and DNA was sonicated into fragments with an average size of around 500 bp. Next, 4 μg H3K27ac antibody (Abcam cat no. ab4729) was used to immunoprecipitate histone H3 acetylated on lysine 27 and associated DNA. DNA was purified using a PCR purification column (Qiagen). ChIP-seq DNA libraries were prepared using a NEBNext Ultra II DNA Library Prep kit (E7645S). DNA libraries were sequenced on the Illumina platform.

CRISPRi and CRISPRa. To silence the activity of BILF2 enhancer, CRISPRi was used. In brief, GM12878 and KAI3 cell lines were transduced with lentiviruses expressing dCAS9-KRAB-MeCP2 fusion protein, followed by selection with 5 μg/mL blasticidin for 5 days. Cells stably expressing dCAS9-KRAB-MeCP2 were then transduced by lentiviruses (PXPR-502) expressing sgRNAs (BILF2isg1-F: CACCGTAATTGCAGTGGACCCCGG, BILF2isg1-R: aaacCCGGGGTCCACTGCAATTAC; BILF2isg2-F: CACCGGAACACATATAACTAACGG, BILF2isg2-R: aaacCCGTTAGTTATATGTGTTCC; BILF2isg3-F: CACCGAGCAACATGGAGACCTCGAA, BILF2isg3-R: aaacTTCGAGGTCTCCATGTTGCTC; BILF2isg4-F: CACCGATTAGGCCTAAAGCCACCTG, BILF2isg4-R: aaacCAGGTGGCTTTAGGCCTAATC; BILF2isg5-F: CACCGCCCCTGCAGAGTAATTGCAG, BILF2isg5-F: aaacCTGCAATTACTCTGCAGGGGC). CRISPRa was used to activate BILF2 enhancer. GM12878 stably expressing dcas9-VP64 was made by transducing lentiviruses expressing dcas9-VP64 fusion protein. Lentiviruses expressing sgRNAs were used to transduce GM12878 cells expressing dcas9-VP64.

RT-qPCR. After puromycin selection for 3 days, reverse transcriptase quantitative PCR (RT-qPCR) was used to measure gene expression. Total mRNAs were extracted using a PureLink RNA Mini Kit (Life Technologies, Carlsbad, CA). mRNAs were converted to cDNA using iScript Reverse Transcription SuperMix (Bio-Rad, Hercules, CA). cDNAs were diluted 20 times with RNase-free H_2O before amplified on an CFX96 Touch real-time PCR detection system (Bio-Rad). SYBR Green (Thermo Fisher Scientific) was used to detect cDNA amplification. GAPDH (glyceraldehyde-3-phosphate dehydrogenase) was used to normalize gene expression. RNA relative expression was calculated using the threshold cycle ($2^{-\Delta\Delta CT}$) method. The value for the cells transduced with non-targeting sgRNA was set to 1. The primer pairs qRT-BARF1-F, GGCTGTCACCGCTTTCTTGG; qRT-BARF1-R, AGGTGTTGGCACTTCTGTGG; qRT-BILF2-F, TCTAAACGTCCCACGCATAAG; qRT-BILF2-R, CCACAGCACAAGTGATTAGGA; qRT-LMP1-F, GCCCTTTGTATACTCCTACTGATG; qRT-LMP1-R, AGACAAGTAAGCACCCGAAGAT; qRT-BALF2-F1, CCGGGCTTCAGCATCAAT; and qRT-BALF2-R1, GGCATTGTGGAACACGTAGA were used to measure BILF2, BALF2, BARF1, and LMP1 expression, respectively. The primer pairs qRT-BALF4-F, CGATGAGGGAGGTGTTTAGTG; qRT-BALF4-R, GATCCACGTCTACAACGACTAC; qRT-BALF5-F, GCAAAGAGGCGAGGAATCT; qRT-BALF5-R, GACTACAAGCTGGACACAGTAG; qRT-BILF1-F, TCAGGTACAGGCACACATTTC, and qRT-BILF1-R, CGTATGGACTCACTTGGGTATG were used to measure BILF2, BALF2, and BARF1.

Data analysis. HiChIP paired-end reads were mapped to human (hg19) and EBV (Akata) genomes using HiC-Pro v2.11.133 (default settings with LIGATION_SITE set as GATCGATC for Mbo I). Due to the small genome size and densely located genes on the EBV genome, we examined EBV chromatin interactions based on genomic bins instead of anchors. In brief, the EBV genome was divided into 1-kb consecutive windows. HiChIP paired-end reads with both ends mapped to EBV genome were counted as bin interactions for two paired bins if the two read ends were located in the two bins separately. The interaction count table based on pairwise bins consisting of all cell lines was first filtered to keep only bin pairs with at least one interaction in one cell line, and was then normalized using the Voom tool with the "quantile" option to account for the sparsity

and dispersion variations in count-based data. Circos plots were generated based on the normalized interaction frequency of 4 or above, which account for the top ~1% of pairwise bin interactions.

SUPPLEMENTAL MATERIAL

Supplemental material is available online only.

SUPPLEMENTAL FILE 1, PDF file, 0.5 MB.

ACKNOWLEDGMENTS

We thank Eric Johannsen and Italo Tempera for advice on the EBV annotation track. We also thank Norio Shimizu for providing SNT13 and SNT16 cells.

This work was supported by grants from the NIH (R01AI123420 and R01CA047006 to B.Z., R01AI164709 to B.G., and 5K99DE030215 to C.W.), JSPS KAKENHI (JP21K15448 to Y.S.), JST (JPMJPR19H5 to Y.S.), AMED (JP19jk0210023 and JP21wm0325042 to Y.S.), the MSD Life Science Foundation (to Y.S.), and a U.S.-Japan Cooperative Medical Sciences Program Collaborative Award from CRDF Global (no. 65604 to B.Z. and Y.S.).

W.D., M.T., and S.J. performed computational work. C.W., Y.N., H.W., M.L., A.H., Y.L., and Y.O. performed experimental work. H.K. and B.G. provided research tool. All other authors contributed significantly to computational, experimental, and/or conceptual development of this work. S.J., Y.S., and B.Z. supervised the project. B.Z. conceptualized the study and wrote the manuscript.

The authors have no competing interests to declare.

REFERENCES

1. Epstein MA, Achong BG, Barr YM. 1964. Virus particles in cultured lymphoblasts from Burkitt's lymphoma. Lancet 283:702–703. https://doi.org/10.1016/S0140-6736(64)91524-7.
2. Longnecker RK, Cohen JI. 2013. Epstein-Barr virus, 8th ed, vol 2. Lippincott Williams & Wilkins, Philadelphia, PA.
3. Cohen JI, Fauci AS, Varmus H, Nabel GJ. 2011. Epstein-Barr virus: an important vaccine target for cancer prevention. Sci Transl Med 3:107fs7. https://doi.org/10.1126/scitranslmed.3002878.
4. Kirchmaier AL, Sugden B. 1995. Plasmid maintenance of derivatives of oriP of Epstein-Barr virus. J Virol 69:1280–1283. https://doi.org/10.1128/JVI.69.2.1280-1283.1995.
5. Hodin TL, Najrana T, Yates JL. 2013. Efficient replication of Epstein-Barr virus-derived plasmids requires tethering by EBNA1 to host chromosomes. J Virol 87:13020–13028. https://doi.org/10.1128/JVI.01606-13.
6. Wang L, Laing J, Yan B, Zhou H, Ke L, Wang C, Narita Y, Zhang Z, Olson MR, Afzali B, Zhao B, Kazemian M. 2020. Epstein-Barr virus episome physically interacts with active regions of the host genome in lymphoblastoid cells. J Virol 94:e01390-20. https://doi.org/10.1128/JVI.01390-20.
7. Kim KD, Tanizawa H, De Leo A, Vladimirova O, Kossenkov A, Lu F, Showe LC, Noma KI, Lieberman PM. 2020. Epigenetic specifications of host chromosome docking sites for latent Epstein-Barr virus. Nat Commun 11:877. https://doi.org/10.1038/s41467-019-14152-8.
8. Wu H, Kapoor P, Frappier L. 2002. Separation of the DNA replication, segregation, and transcriptional activation functions of Epstein-Barr nuclear antigen 1. J Virol 76:2480–2490. https://doi.org/10.1128/jvi.76.5.2480-2490.2002.
9. Frappier L. 2015. EBNA1. Curr Top Microbiol Immunol 391:3–34. https://doi.org/10.1007/978-3-319-22834-1_1.
10. Wu H, Ceccarelli DF, Frappier L. 2000. The DNA segregation mechanism of Epstein-Barr virus nuclear antigen 1. EMBO Rep 1:140–144. https://doi.org/10.1093/embo-reports/kvd026.
11. Lee MA, Diamond ME, Yates JL. 1999. Genetic evidence that EBNA-1 is needed for efficient, stable latent infection by Epstein-Barr virus. J Virol 73:2974–2982. https://doi.org/10.1128/JVI.73.4.2974-2982.1999.
12. De Leo A, Calderon A, Lieberman PM. 2020. Control of viral latency by episome maintenance proteins. Trends Microbiol 28:150–162. https://doi.org/10.1016/j.tim.2019.09.002.
13. Zhao B, Zou J, Wang H, Johannsen E, Peng CW, Quackenbush J, Mar JC, Morton CC, Freedman ML, Blacklow SC, Aster JC, Bernstein BE, Kieff E. 2011. Epstein-Barr virus exploits intrinsic B-lymphocyte transcription programs to achieve immortal cell growth. Proc Natl Acad Sci U S A 108:14902–14907. https://doi.org/10.1073/pnas.1108892108.
14. Harada S, Kieff E. 1997. Epstein-Barr virus nuclear protein LP stimulates EBNA-2 acidic domain-mediated transcriptional activation. J Virol 71:6611–6618. https://doi.org/10.1128/JVI.71.9.6611-6618.1997.
15. Ohashi M, Hayes M, McChesney K, Johannsen E. 2021. Epstein-Barr virus nuclear antigen 3C (EBNA3C) interacts with the metabolism sensing C-terminal binding protein (CtBP) repressor to upregulate host genes. PLoS Pathog 17:e1009419. https://doi.org/10.1371/journal.ppat.1009419.
16. Wang LW, Jiang S, Gewurz BE. 2017. Epstein-Barr virus LMP1-mediated oncogenicity. J Virol 91:e01718-16. https://doi.org/10.1128/JVI.01718-16.
17. Cen O, Longnecker R. 2015. Latent Membrane Protein 2 (LMP2). Curr Top Microbiol Immunol 391:151–180. https://doi.org/10.1007/978-3-319-22834-1_5.
18. Lee N, Moss WN, Yario TA, Steitz JA. 2015. EBV noncoding RNA binds nascent RNA to drive host PAX5 to viral DNA. Cell 160:607–618. https://doi.org/10.1016/j.cell.2015.01.015.
19. Szymula A, Palermo RD, Bayoumy A, Groves IJ, Ba Abdullah M, Holder B, White RE. 2018. Epstein-Barr virus nuclear antigen EBNA-LP is essential for transforming naive B cells, and facilitates recruitment of transcription factors to the viral genome. PLoS Pathog 14:e1006890. https://doi.org/10.1371/journal.ppat.1006890.
20. Sharp TV, Schwemmle M, Jeffrey I, Laing K, Mellor H, Proud CG, Hilse K, Clemens MJ. 1993. Comparative analysis of the regulation of the interferon-inducible protein kinase PKR by Epstein-Barr virus RNAs EBER-1 and EBER-2 and adenovirus VAI RNA. Nucleic Acids Res 21:4483–4490. https://doi.org/10.1093/nar/21.19.4483.
21. Li Z, Tsai MH, Shumilov A, Baccianti F, Tsao SW, Poirey R, Delecluse HJ. 2019. Epstein-Barr virus ncRNA from a nasopharyngeal carcinoma induces an inflammatory response that promotes virus production. Nat Microbiol 4:2475–2486. https://doi.org/10.1038/s41564-019-0546-y.
22. Skinner CM, Ivanov NS, Barr SA, Chen Y, Skalsky RL. 2017. An Epstein-Barr virus microRNA blocks interleukin-1 (IL-1) signaling by targeting IL-1 receptor 1. J Virol 91:e00530-17. https://doi.org/10.1128/JVI.00530-17.
23. Pich D, Mrozek-Gorska P, Bouvet M, Sugimoto A, Akidil E, Grundhoff A, Hamperl S, Ling PD, Hammerschmidt W. 2019. First days in the life of naive human B lymphocytes infected with Epstein-Barr virus. mBio 10:e01723-19. https://doi.org/10.1128/mBio.01723-19.
24. Arvey A, Tempera I, Tsai K, Chen HS, Tikhmyanova N, Klichinsky M, Leslie C, Lieberman PM. 2012. An atlas of the Epstein-Barr virus transcriptome and epigenome reveals host-virus regulatory interactions. Cell Host Microbe 12:233–245. https://doi.org/10.1016/j.chom.2012.06.008.
25. Chen HS, Martin KA, Lu F, Lupey LN, Mueller JM, Lieberman PM, Tempera I. 2014. Epigenetic deregulation of the LMP1/LMP2 locus of Epstein-Barr virus

by mutation of a single CTCF-cohesin binding site. J Virol 88:1703–1713. https://doi.org/10.1128/JVI.02209-13.
26. Frappier L, Goldsmith K, Bendell L. 1994. Stabilization of the EBNA1 protein on the Epstein-Barr virus latent origin of DNA replication by a DNA looping mechanism. J Biol Chem 269:1057–1062. https://doi.org/10.1016/S0021-9258(17)42220-4.
27. Morgan SM, Tanizawa H, Caruso LB, Hulse M, Kossenkov A, Madzo J, Keith K, Tan Y, Boyle S, Lieberman PM, Tempera I. 2022. The three-dimensional structure of Epstein-Barr virus genome varies by latency type and is regulated by PARP1 enzymatic activity. Nat Commun 13:187. https://doi.org/10.1038/s41467-021-27894-1.
28. Kim TH, Abdullaev ZK, Smith AD, Ching KA, Loukinov DI, Green RD, Zhang MQ, Lobanenkov VV, Ren B. 2007. Analysis of the vertebrate insulator protein CTCF-binding sites in the human genome. Cell 128:1231–1245. https://doi.org/10.1016/j.cell.2006.12.048.
29. Zhang Y, Zhang X, Dai HQ, Hu H, Alt FW. 2022. The role of chromatin loop extrusion in antibody diversification. Nat Rev Immunol. https://doi.org/10.1038/s41577-022-00679-3.
30. Davidson IF, Peters JM. 2021. Genome folding through loop extrusion by SMC complexes. Nat Rev Mol Cell Biol 22:445–464. https://doi.org/10.1038/s41580-021-00349-7.
31. Tempera I, Klichinsky M, Lieberman PM. 2011. EBV latency types adopt alternative chromatin conformations. PLoS Pathog 7:e1002180. https://doi.org/10.1371/journal.ppat.1002180.
32. Tempera I, Wiedmer A, Dheekollu J, Lieberman PM. 2010. CTCF prevents the epigenetic drift of EBV latency promoter Qp. PLoS Pathog 6:e1001048. https://doi.org/10.1371/journal.ppat.1001048.
33. Chau CM, Zhang XY, McMahon SB, Lieberman PM. 2006. Regulation of Epstein-Barr virus latency type by the chromatin boundary factor CTCF. J Virol 80:5723–5732. https://doi.org/10.1128/JVI.00025-06.
34. Dekker J, Rippe K, Dekker M, Kleckner N. 2002. Capturing chromosome conformation. Science 295:1306–1311. https://doi.org/10.1126/science.1067799.
35. Lieberman-Aiden E, van Berkum NL, Williams L, Imakaev M, Ragoczy T, Telling A, Amit I, Lajoie BR, Sabo PJ, Dorschner MO, Sandstrom R, Bernstein B, Bender MA, Groudine M, Gnirke A, Stamatoyannopoulos J, Mirny LA, Lander ES, Dekker J. 2009. Comprehensive mapping of long-range interactions reveals folding principles of the human genome. Science 326:289–293. https://doi.org/10.1126/science.1181369.
36. Wood CD, Veenstra H, Khasnis S, Gunnell A, Webb HM, Shannon-Lowe C, Andrews S, Osborne CS, West MJ. 2016. MYC activation and BCL2L11 silencing by a tumour virus through the large-scale reconfiguration of enhancer-promoter hubs. Elife 5:e18270. https://doi.org/10.7554/eLife.18270.
37. Mumbach MR, Rubin AJ, Flynn RA, Dai C, Khavari PA, Greenleaf WJ, Chang HY. 2016. HiChIP: efficient and sensitive analysis of protein-directed genome architecture. Nat Methods 13:919–922. https://doi.org/10.1038/nmeth.3999.
38. Munschauer M, Nguyen CT, Sirokman K, Hartigan CR, Hogstrom L, Engreitz JM, Ulirsch JC, Fulco CP, Subramanian V, Chen J, Schenone M, Guttman M, Carr SA, Lander ES. 2018. The NORAD lncRNA assembles a topoisomerase complex critical for genome stability. Nature 561:132–136. https://doi.org/10.1038/s41586-018-0453-z.
39. Okuno Y, Murata T, Sato Y, Muramatsu H, Ito Y, Watanabe T, Okuno T, Murakami N, Yoshida K, Sawada A, Inoue M, Kawa K, Seto M, Ohshima K, Shiraishi Y, Chiba K, Tanaka H, Miyano S, Narita Y, Yoshida M, Goshima F, Kawada JI, Nishida T, Kiyoi H, Kato S, Nakamura S, Morishima S, Yoshikawa T, Fujiwara S, Shimizu N, Isobe Y, Noguchi M, Kikuta A, Iwatsuki K, Takahashi Y, Kojima S, Ogawa S, Kimura H. 2019. Defective Epstein-Barr virus in chronic active infection and haematological malignancy. Nat Microbiol 4:404–413. https://doi.org/10.1038/s41564-018-0334-0.
40. Zhang Y, Ohyashiki JH, Takaku T, Shimizu N, Ohyashiki K. 2006. Transcriptional profiling of Epstein-Barr virus (EBV) genes and host cellular genes in nasal NK/T-cell lymphoma and chronic active EBV infection. Br J Cancer 94:599–608. https://doi.org/10.1038/sj.bjc.6602968.
41. Chiang AK, Tao Q, Srivastava G, Ho FC. 1996. Nasal NK- and T-cell lymphomas share the same type of Epstein-Barr virus latency as nasopharyngeal carcinoma and Hodgkin's disease. Int J Cancer 68:285–290. https://doi.org/10.1002/(SICI)1097-0215(19961104)68:3%3C285::AID-IJC3%3E3.0.CO;2-Y.
42. Xiong J, Cui BW, Wang N, Dai YT, Zhang H, Wang CF, Zhong HJ, Cheng S, Ou-Yang BS, Hu Y, Zhang X, Xu B, Qian WB, Tao R, Yan F, Hu JD, Hou M, Ma XJ, Wang X, Liu YH, Zhu ZM, Huang XB, Liu L, Wu CY, Huang L, Shen YF, Huang RB, Xu JY, Wang C, Wu DP, Yu L, Li JF, Xu PP, Wang L, Huang JY, Chen SJ, Zhao WL. 2020. Genomic and transcriptomic characterization of natural killer T cell lymphoma. Cancer Cell 37:403–419.e6. https://doi.org/10.1016/j.ccell.2020.02.005.
43. Tsuge I, Morishima T, Morita M, Kimura H, Kuzushima K, Matsuoka H. 1999. Characterization of Epstein-Barr virus (EBV)-infected natural killer (NK) cell proliferation in patients with severe mosquito allergy; establishment of an IL-2-dependent NK-like cell line. Clin Exp Immunol 115:385–392. https://doi.org/10.1046/j.1365-2249.1999.00836.x.
44. Oyoshi MK, Nagata H, Kimura N, Zhang Y, Demachi A, Hara T, Kanegane H, Matsuo Y, Yamaguchi T, Morio T, Hirano A, Shimizu N, Yamamoto K. 2003. Preferential expansion of Vgamma9-JgammaP/Vdelta2-Jdelta3 gammadelta T cells in nasal T-cell lymphoma and chronic active Epstein-Barr virus infection. Am J Pathol 162:1629–1638. https://doi.org/10.1016/s0002-9440(10)64297-6.
45. Klein G, Teramoto N, Manneborg-Sandlund A, Lennette ET, Chen F, Szeles A, Löwbeer M, Szekely L, Pokrovskaja K, Ehlin-Henriksson B. 1998. Restricted expression of Epstein-Barr virus (EBV)-encoded, growth transformation-associated antigens in an EBV- and human herpesvirus type 8-carrying body cavity lymphoma line. J Gen Virol 79:1445–1452. https://doi.org/10.1099/0022-1317-79-6-1445.